High-pressure structure and elastic properties of tantalum single crystal: First principles investigation*

Jian-Bing Gu(顾建兵)[1], Chen-Ju Wang(王臣菊)[1,†], Wang-Xi Zhang(张旺玺)[1], Bin Sun(孙斌)[1], Guo-Qun Liu(刘国群)[1], Dan-Dan Liu(刘丹丹)[2], and Xiang-Dong Yang(杨向东)[3]

[1] *School of Materials and Chemical Engineering, Zhongyuan University of Technology, Zhengzhou* 450007, *China*
[2] *College of Science, Zhongyuan University of Technology, Zhengzhou* 450007, *China*
[3] *Institute of Atomic and Molecular Physics, Sichuan University, Chengdu* 610065, *China*

(Received 12 May 2016; revised manuscript received 3 August 2016; published online 25 October 2016)

Since knowledge of the structure and elastic properties of Ta at high pressures is critical for addressing the recent controversies regarding the high-pressure stable phase and elastic properties, we perform a systematical study on the high-pressure structure and elastic properties of the cubic Ta by using the first-principles method. Results show that the initial body-centered cubic phase of Ta remains stable even up to 500 GPa and the high-pressure elastic properties are excellently consistent with the available experimental results. Besides, the high-pressure sound velocities of the single- and poly-crystals Ta are also calculated based on the elastic constants, and the predications exhibit good agreement with the existing experimental data.

Keywords: high-pressure structure, elastic properties, sound velocities, density functional theory

PACS: 61.50.–f, 71.15.Mb, 43.35.+d, 31.15.E– **DOI:** 10.1088/1674-1056/25/12/126103

1. Introduction

Tantalum, as an important pressure standard, is always largely compressed under very high pressure. To have an insight into its phase transition mechanism and mechanical stability under extreme conditions, investigations on the high-pressure structure and elastic properties of Ta are essential.

Although a great deal of effort both in experimental[1–10] and theoretical[11–15] fields has been put into the high-pressure structure of Ta, discrepancies on the stable structure at high pressures remain inconclusive up to now. For example, the shock wave experiments[1–3] indicated the body-centered cubic (bcc) structure would transform into the hexagonal phase at 45 GPa, while recent first-principles simulation[11] showed this phase transition occurred above 70 GPa. Surprisingly, the diamond-anvil cell (DAC) experiments[4–7] showed the bcc structure remained stable up to 135 GPa[4] and 174 GPa,[5–7] respectively. Besides, other shock experimental[8–10] and theoretical[12–15] research indicated that the bcc phase was still stable under pressure up to 500 GPa. In addition, many experiments[16–18] were also performed to determine the high-pressure elastic properties of the Ta since the ultrasonic experiment first measured its elastic moduli at pressure up to 0.5 GPa.[19] For instance, the impulsive stimulated light scattering (ISLS) measurement carried out by Crowhurst *et al.*[16] gave the results up to 30 GPa and radial x-ray diffraction measurement (RXRD) fulfilled by Cynn and Yoo[17] yielded the data up to 105 GPa. Furthermore, inelastic x-ray scattering (IXS) accomplished by Antonangeli *et al.*[18] provided the results up to 120 GPa. Simultaneously, the high-pressure elastic constants of Ta were also predicated by several theoretical calculations.[20–26] Unfortunately, we find that some disagreements exist among the results of the elastic constants above 20 GPa. All these discrepancies described above motivate us to further investigate the high-pressure stable structure and elastic properties of the Ta.

In the present paper, we perform a systematical investigation of the high-pressure structure and elastic properties of the Ta by using the first-principles calculations. The rest of this article is organized as follows. In Section 2, we present the details of the calculations. Results and discussion are given in Section 3. Conclusions of this work are drawn in Section 4.

2. Computational details

2.1. Total energy calculations

The zero-temperature energies of the bcc, fcc, and hcp structures of the Ta in the pressure range of 0 GPa–500 GPa are calculated by the Vienna *ab initio* simulation package VASP code.[27–30] The generalized gradient approximation (GGA) in

*Project supported by the Basic and Frontier Technical Research Project of Henan Province, China (Grant No. 152300410228), the University Innovation Team Project in Henan Province, China (Grant No. 15IRTSTHN004), and the Key Scientific Research Project of Higher Education of Henan Province, China (Grant No. 17A140014).

†Corresponding author. E-mail: scu_wcj@163.com

© 2016 Chinese Physical Society and IOP Publishing Ltd

the Perdew–Burke–Ernzerhof parameterization (PBE)[31–34] is chosen to treat the exchange–correlation effects. Specifically, the projector augmented-wave (PAW) potential[35] with 11 valence electrons $5p^6 6s^2 5d^3$ is used.

In addition, energy convergence (1 meV per atom) tests at 0 GPa are performed to determine the cutoff energy and the number of *k*-points. As displayed in Fig. 1, all the energies converged well for the bcc, fcc, and hcp phases after the cutoff energy reached 500 eV. From Fig. 2, we can clearly see that the all the energies show a good convergence when the *k*-points mesh size reaches 18×18×18 for the bcc and fcc phases and 15×15×11 for the hcp phase, respectively. Besides, similar energy convergence tests are also performed at 500 GPa to guarantee the correct predictions at high pressures.

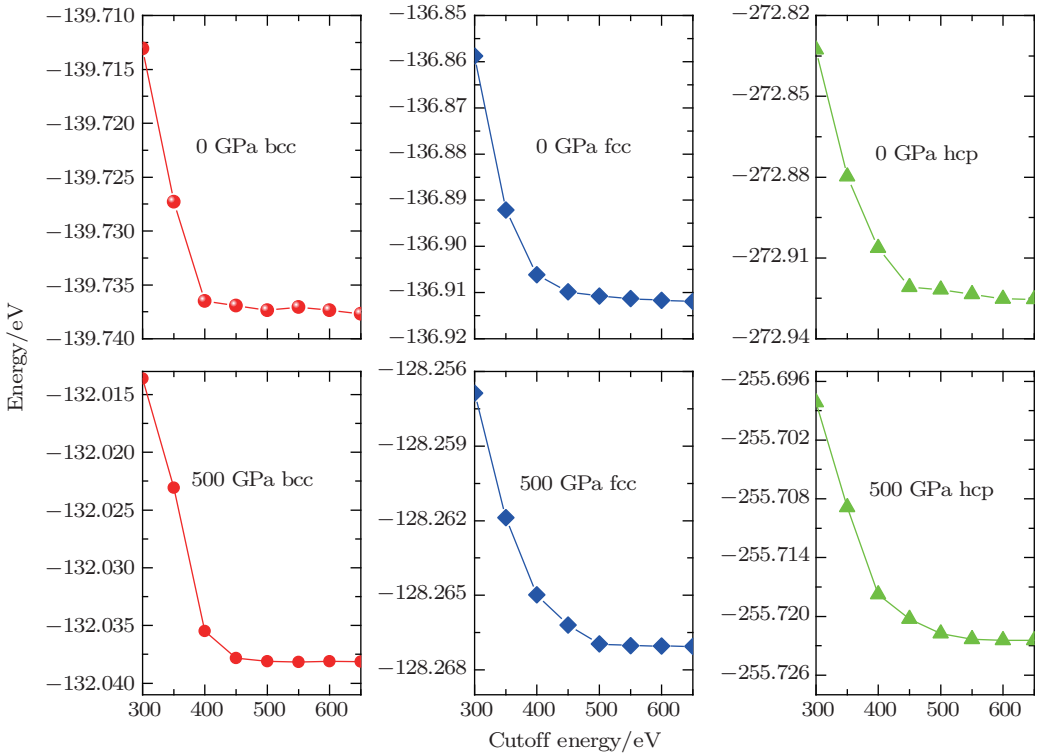


Fig. 1. (color online) Energy convergence tests of the cutoff energy at 0 GPa and 500 GPa respectively for the bcc, fcc, and hcp phases.

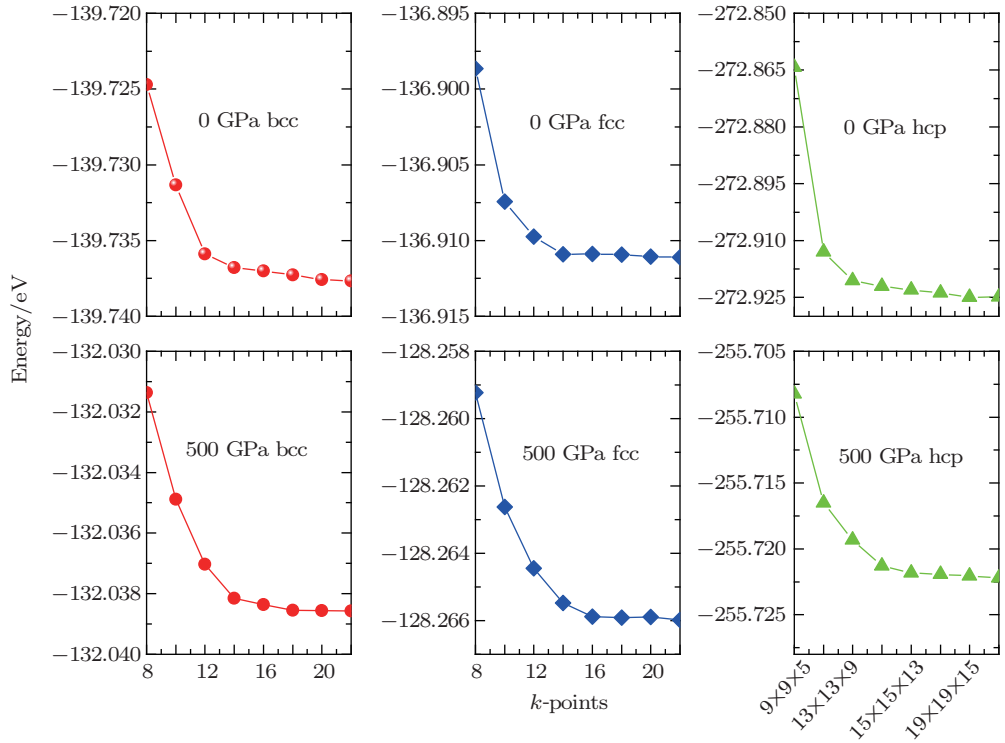


Fig. 2. (color online) Energy convergence tests of the k-points respectively at 0 GPa and 500 GPa for the bcc, fcc, and hcp phases.

As presented in Figs. 1 and 2, the cutoff energy 500 eV and k-points (18×18×18 for bcc and fcc, and 15×15×11 for hcp Ta) ascertained at 0 GPa are also suitable for those of the high pressure. Therefore, the reasonable cutoff energy 500 eV and rational k-points (18×18×18 for bcc and fcc, and 15×15×11 for hcp Ta) are used in the present calculations. Based on the total energies at various volumes, the equation of state of the bcc Ta at 0 K can be determined by fitting the fourth-order Brich–Murnaghan equation[36] $E(V) = \sum_{n=1}^{4} a_n V^{-2n/3}$. Then the P–V data can be obtained directly from $P = -(\partial E/\partial V)_{T=0}$, which is the basis of the elastic constants calculations at different pressures. In addition, the bulk modulus can be calculated from $B_{\mathrm{T}} = V\partial^2 E/\partial V^2$, and its pressure derivative can be obtained by $B'_{\mathrm{T}} = \mathrm{d}B_{\mathrm{T}}/\mathrm{d}P$.

2.2. Elastic properties calculations

In the present work, the single-crystal elastic constants C_{11}, C_{12}, and C_{44} of the Ta are calculated by taking the second derivatives of the free energies with respect to strain tensor. To determine the elastic constants C_{11} and C_{12}, we adopt the volume conserving deformation gradient matrix (1), which is ensured by $\det[\alpha_{ij}] = 1$.

$$\alpha_{ij} = \begin{pmatrix} 1+\delta & 0 & 0 \\ 0 & 1-\delta & 0 \\ 0 & 0 & 1/(1-\delta^2) \end{pmatrix}, \tag{1}$$

where δ is the strain magnitude, and it is set from -0.006 to 0.006 in steps of 0.001. The corresponding energies can be expressed as

$$E(\delta) = E(0) + (C_{11} - C_{12} - 2P)V\delta^2 + 0(\delta^3), \tag{2}$$

with $E(\delta)$ and $E(0)$ respectively representing the energy of the deformed and undeformed unit cell, V denoting the volume, P standing for the pressure applied on the reference state. Then the value of $C_{11} - C_{12}$ can be deduced from a least-squares fit of formula (2). To calculate the C_{11} and C_{12} respectively, the relationship between the elastic constants and bulk modulus

$$B_{\mathrm{T}} = \frac{C_{11} + 2C_{12} + P}{3} \tag{3}$$

is used.

In addition, the volume conserving deformation gradient matrix (4) is used to calculate the C_{44}

$$\alpha_{ij} = \begin{pmatrix} 1 & 0 & \delta \\ 0 & 1/(1-\delta^2) & 0 \\ \delta & 0 & 1 \end{pmatrix}. \tag{4}$$

The corresponding energy expression is

$$E(\delta) = E(0) + (2C_{44} - 2P)V\delta^2 + 0(\delta^4). \tag{5}$$

Since the stress–strain coefficients defined as the first derivative of the stress with respect to strain are the felicitous quantities which describe the elastic properties of a system under the isotropic pressure, the elastic constants are transformed into the corresponding stress–strain coefficients by the following expressions[37]

$$B_{11} = C_{11} - P, \quad B_{12} = C_{12} + P, \quad \text{and} \quad B_{44} = C_{44} - P. \tag{6}$$

For polycrystalline materials, the isotropic average bulk and shear moduli can be determined according to the Voigt–Reuss–Hill approximations[38] $B_{\mathrm{T}} = (B_V + B_R)/2$ and $G = (G_V + G_R)/2$, where B_V, B_R, G_V, and G_R are expressed respectively as

$$B_V = B_R = \frac{B_{11} + 2B_{12}}{3}, \tag{7}$$

$$G_V = \frac{1}{5}(B_{11} - B_{12} + 3B_{44}), \tag{8}$$

and

$$G_R = \frac{5(B_{11} - B_{12})B_{44}}{3(B_{11} - B_{12}) + 4B_{44}}. \tag{9}$$

Based on the values of the isotropic average bulk and shear moduli, we also calculate the Young's modulus Y and Poisson's modulus ν by the following formulas

$$Y = \frac{9BG}{3B + G} \quad \text{and} \quad \nu = \frac{3B - 2G}{2(3B + G)} = \frac{1}{2}\left(1 - \frac{Y}{3B}\right). \tag{10}$$

2.3. Sound velocities

Sound velocities of the single-crystal Ta can be obtained through the Christoffel equation[39]

$$\det\left|B_{ijkl} n_j n_l - \rho V^2 \delta_{ik}\right| = 0, \tag{11}$$

where ρ is the mass density, n_j and n_l represent the direction cosines of the sound wave, V denotes the sound velocity, B_{ijkl} stands for the stress–strain coefficients tensor under isotropic pressure, and δ_{ik} is the Kronecker delta. For [110] wave propagation direction in the single-crystal Ta, the longitudinal sound velocity can be obtained by the following formula

$$V_{[110]} = \sqrt{\frac{c_{11} + c_{12} + 2c_{44}}{2\rho}}. \tag{12}$$

Its two transverse sound velocities respectively along [001] and $[1\bar{1}0]$ directions can be calculated by the equations

$$V_{[001]} = \sqrt{\frac{c_{44}}{\rho}} \tag{13}$$

and

$$V_{[1\bar{1}0]} = \sqrt{\frac{c_{11} - c_{12}}{2\rho}}. \tag{14}$$

For the polycrystalline Ta, the isotropic average aggregate velocities can be calculated through the following three expressions

$$V_P = \left(\frac{B_{\rm T} + 4G/3}{\rho}\right)^{1/2}, \tag{15}$$

$$V_B = \left(\frac{B_{\rm T}}{\rho}\right)^{1/2}, \tag{16}$$

and

$$V_S = \left(\frac{G}{\rho}\right)^{1/2}. \tag{17}$$

Where V_P, V_S, and V_B respectively represent the compression, shear and bulk sound velocities, $B_{\rm T}$ and G are the isotropic average bulk and shear moduli of the polycrystalline Ta.

3. Results and discussion

3.1. Equilibrium structure and equation of state

To verify the accuracy of the present calculations, we list the calculated equilibrium lattice parameter a, bulk modulus B_0 and its pressure derivative B_0' of the bcc Ta in Table 1, together with the available experimental results.[17,40,41]

Table 1. Calculated equilibrium lattice parameters a (in unit Å), bulk modulus B_0 (in unit GPa) and its pressure derivatives B_0', together with the experimental results.[17,40,41] GGA-PBE: generalized gradient approximation-Perdew–Burke–Ernzerhof, XRD: x-ray diffraction, DAC: diamond anvil cell.

	Method	a/Å	B_0/GPa	B_0'
Ta	Present work (GGA-PBE)	3.322	195	3.47
	Expt.[17] (XRD in DAC)	3.304	194	3.55
	Expt.[40] (XRD in DAC)	3.304	194	3.52
	Expt.[41] (XRD in DAC)	3.304	195	3.40

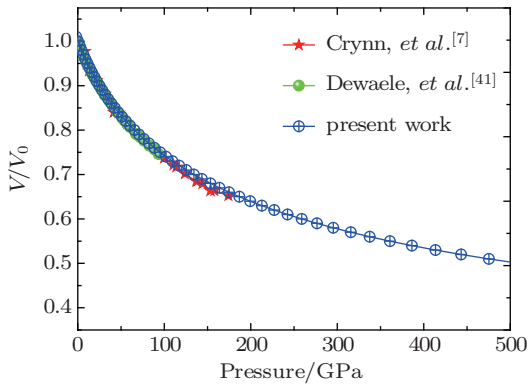


Fig. 3. (color online) Relative volumeV/V_0 as a function of pressure, compared with the existing experimental results.[7,42]

From Table 1, we can clearly see that the calculated lattice parameter of the bcc Ta is in fair agreement (within 0.5%) with the experimental data.[17,40,41] In addition, the bulk modulus and its pressure derivative are also in good agreement with the existing experimental results.[40,41] Besides, the pressure dependence of the relative volume V/V_0 is also displayed in Fig. 3, together with the available experimental data.[7,42] From Fig. 3, we find that the agreement of the P–V/V_0 curve and the experimental results[7,42] is rather satisfactory. The agreement mentioned above indicates that the choice of the PAW pseudopotential and GGA-PBE approximation is reasonable for the current study and the present calculations are reliable.

To decide the stable structure of the single crystal Ta at high pressures, we calculate the enthalpies $H = E + PV$ as a function of pressure for the bcc, fcc, and hcp phases at zero-temperature and display the enthalpy differences relative to the bcc structure in Fig. 4. The positive of the enthalpy differences shown in Fig. 4 implies that the bcc structure of the Ta is the most stable structure in the studied pressure range of 0 GPa to 500 Gpa. This is consistent with the experimental discoveries[8–10] and other theoretical results.[12–15]

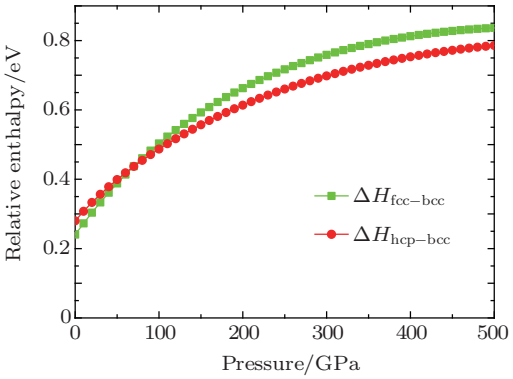


Fig. 4. (color online) Pressure dependence of the enthalpy differences ΔH of the fcc and hcp structures with respect to the bcc phase of the single crystal Ta.

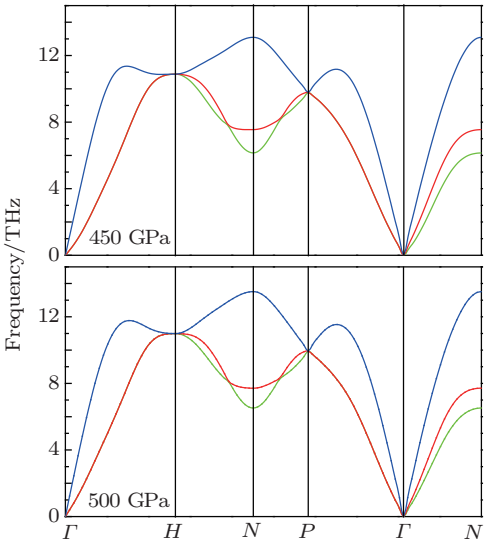


Fig. 5. (color online) Phonon dispersion curves of the bcc phase of the Ta single crystal respectively at 450 GPa and 500 GPa.

To further test the dynamic stability of the bcc structure of the Ta single crystal at high pressures, we also calculate

the phonon dispersion curves of the bcc phase respectively at 450 GPa and 500 GPa by using the method described in Refs. [43] and [44]. As displayed in Fig. 5, the imaginary frequency is not presented in the whole pressure range. This indicates that the bcc structure of the Ta is dynamically stable up to 500 GPa at 0 K. Therefore, the following results and discussion are fulfilled only based on the bcc phase of the Ta single crystal. Based on the conclusion, we list the high-pressure lattice constants and corresponding volumes of the bcc structure obtained in the present work in Table 2, and hope that the predicted results can serve as a valuable guidance or reference for further related investigations which will be conducted someday.

Table 2. Predicted high-pressure lattice constants a and corresponding volumes V of the bcc phase of the Ta single crystal.

Pressure	0	100	200	300	400	500
a/Å	3.322	3.009	2.862	2.767	2.697	2.642
V/Å^3	18.330	13.622	11.721	10.592	9.809	9.221

3.2. Elastic properties

The pressure dependence of the calculated stress–strain coefficients describing the elastic properties of materials under isotropic pressure are displayed in Fig. 6(a). From Fig. 6(a), we find that the calculated stress–strain coefficients B_{11}, B_{12}, and B_{44} not only show an upward tendency with pressure increasing, but also reveal good agreement with the available experimental values[17,45] at high pressures. In addition, we also find that the effect of the pressure on B_{11} is much larger than that on B_{12} and B_{44}. This may originate from the fact that the stress–strain coefficient B_{11} representing the elasticity in length changes with longitudinal strain, while B_{12} and B_{44} are related to the elasticity in shape. A transverse strain causes a change in shape at a constant volume. Therefore, B_{12} and B_{44} are less sensitive to pressure than that of the B_{11}.

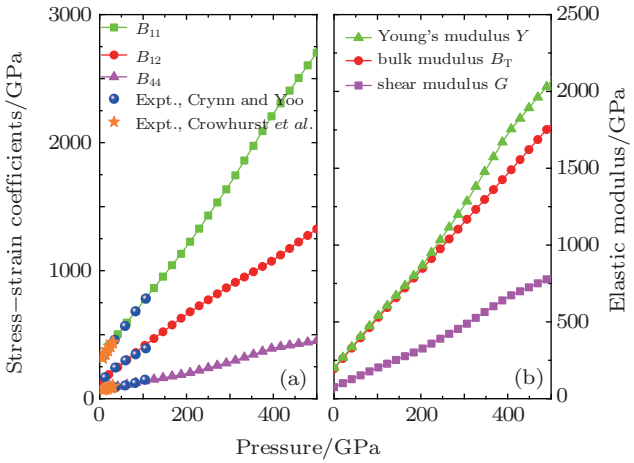


Fig. 6. (color online) (a) Calculated stress–strain coefficients of the bcc Ta versus pressure at 0 K, together with the corresponding experimental results.[17,45] (b) Bulk, Young's, and shear modulus of the polycrystalline Ta versus pressure at 0 K.

Since the bulk and shear modulus respectively represent the resistance to fracture and plastic deformation of a material, they are calculated and displayed in Fig. 6(b). Figure 6(b) shows that both the bulk and shear modulus present an increasing change tendency with the enhancement of pressure. Based on the calculated bulk and shear modulus, we analyze the high-pressure ductility or brittle nature of the bcc Ta according to the Pugh criterion.[46] Generally, materials become more and more ductile with pressure increasing. Moreover, the material behaves in a ductile manner when B/G is above 1.75; otherwise it exhibits a brittle nature. In the case of the bcc Ta, Fig. 7 shows that each value of the B/G is larger than 1.75. Consequently, the bcc Ta can be regarded as a ductile material in the whole studied pressure range.

Young's modulus Y and Poisson's ratio v characterizing the elastic properties of a material are important physical quantities. Specifically, Young's modulus often provides a criterion of stiffness of a solid, i.e., the larger the value of Y, the stiffer is the material. Poisson's ratio reveals the brittleness and ductility of a material. According to Frantsevich's rule,[47] the critical value of Poisson ratio of a material is 1/3. For brittle materials, the Poisson ratio is less than 1/3. Otherwise, materials are ductile. As clearly displayed in Fig. 7, all the calculated Poisson ratios of the bcc Ta are larger than 1/3 in the studied pressure range, so the bcc Ta is regarded as a ductile material. The result is excellently consistent with the conclusion obtained from the Poisson ratio.

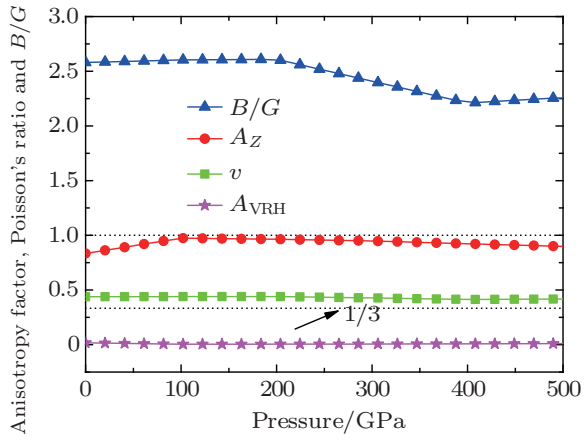


Fig. 7. (color online) Pressure dependence of the anisotropy factors A_Z and A_{VRH}, Poisson's ratio v, and B/G ratio.

On the basis of the elastic properties described above, we further probe the mechanical stability of the bcc Ta under high pressure by using the generalized elastic stability criteria

$$B_{11}+2B_{12}>0, \quad B_{44}>0, \quad B_{11}-B_{12}>0. \tag{18}$$

Obviously, all the above restrictions are satisfied in the studied pressure range, which again implies that the bcc structure of the Ta single crystal is mechanically stable at least up to 500 GPa.

3.3. Elastic anisotropy

Elastic anisotropy of a crystal is the orientation dependence of the elastic moduli. Essentially, the elastic properties of all single crystals are anisotropic. Therefore, it is necessary to explore the anisotropy of crystals when we study their elastic properties. The anisotropy factors

$$A_Z = \frac{2C_{44}}{C_{11}-C_{12}} \quad \text{and} \quad A_{\rm VRH} = \frac{G_V - G_R}{G_V + G_R} \tag{19}$$

respectively introduced by Zener[48] and Chung *et al.*[49] are usually used to quantify the elastic anisotropy of cubic crystals. For an isotropic crystal, A_Z equals 1, otherwise the material is anisotropic. The magnitude of a deviation from 1 is a measure of the degree of elastic anisotropy possessed by the crystal. Simultaneously, a material is isotropic when $A_{\rm VRH}$ equals 0, otherwise it is anisotropic. From Fig. 7, we can clearly see that the value of the anisotropy factors A_Z and $A_{\rm VRH}$ respectively approaches 1 and 0. Moreover, both of them vary very slightly with pressure, which suggests that the Ta is nearly isotropic in the whole studied pressure range.

3.4. Sound velocities

According to Eqs. (12)–(14), we calculate the longitudinal and transverse sound velocities $V_{[110]}$, $V_{[001]}$, and $V_{[1\bar{1}0]}$ of the [110] wave propagation direction in the single crystal Ta. Meanwhile, the compression, shear and bulk sound velocities V_P, V_S, and V_B of the polycrystalline Ta are also calculated by using formulas (15)–(17). To explore the tendency of these sound velocities of single- and poly-crystal Ta with pressure increasing, the pressure dependence of these sound velocities and available experimental results[17,19,45,50,51] is displayed in Fig. 8. From Fig. 8, we can clearly see that all the sound velocities increase monotonously as the pressure increases in both cases of the single- and poly-crystal Ta. In addition, it is worth pointing out that the compression and bulk sound velocities V_P and V_B of the polycrystalline Ta are in good agreement with the existing experimental results obtained respectively by the radial x-ray diffraction measurement (RXRD),[17] ultrasonic experiment,[19] impulsive stimulated light scattering (ISLS) experiment,[45] and inelastic x-ray scattering (IXS) method.[50,51] Only little division between the experimental data and theoretical values may be originated from the temperature effect, for the experimental results were obtained at the 300 K and the theoretical data is calculated at 0 K. Finally, it should be pointed out that the corresponding theoretical values calculated by other authors are not referred to in the present work, for the results obtained by different numerical procedures and forms of exchange–correlation functional have different accuracy. We deem that it is insignificant to compare our data with other theoretical results.

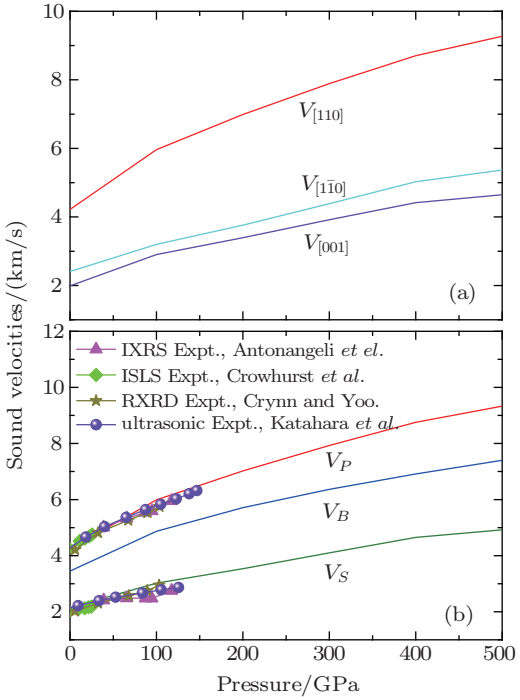


Fig. 8. (color online) Pressure dependence of the sound velocities of the single crystal (a) and polycrystalline (b) Ta, together with the experimental results.[17,19,45,50,51]

4. Conclusion

Investigations of the structure, elastic properties and sound velocities of the Ta single crystal at high pressures are performed by using the first-principles calculations in the present work. It is found that the initial bcc structure under ambient condition remains stable up to 500 GPa at 0 K and the high-pressure elastic properties of the cubic Ta single crystal show excellent agreement with the available experimental results. In addition, the high-pressure mechanical stability of the bcc Ta is also confirmed by the elastic stability criteria of the elastic properties. Finally, the sound velocities of the single- and poly-crystal Ta are also calculated based on the results of the elastic constants. Furthermore, the sound velocities of the polycrystalline Ta are in good consistency with the existing experimental results obtained by various diamond-anvil-cell experiments.

References

[1] Hsiung L M and Lassila D H 2000 *Acta Mater.* **48** 4851
[2] Hsiung L and Lassila D 1998 *Scr. Mater.* **39** 603
[3] Hsiung L L 2010 *J. Phys.: Condens. Matter* **22** 385702
[4] Dewaele A, Mezouar M, Guignot N and Loubeyre P 2010 *Phys. Rev. Lett.* **104** 255701
[5] Errandonea D, Schwager B, Ditz R, Gessmann C, Boehler R and Ross M 2001 *Phys. Rev. B* **63** 132104
[6] Errandonea D, Somayazulu M, Hausermann D and Mao H K 2003 *J. Phys.: Condens. Matter* **15** 7635
[7] Crynn H and Yoo C 1999 *Phys. Rev. B* **59** 8526
[8] Holmes N C, Moriarty J A, Gathers G and Nellis W J 1989 *J. Appl. Phys.* **66** 2962
[9] Nellis W J, Mitchell A C and Young D A 2003 *J. Appl. Phys.* **93** 304
[10] Mitchell A and Nellis W 1981 *J. Appl. Phys.* **52** 3363

[11] Burakovsky L, Chen S P, Preston D L, Belonoshko A B, Rosengren A, Mikhaylushkin A S, Simak S I and Moriarty J A 2010 *Phys. Rev. Lett.* **104** 255702
[12] Moriarty J A 1994 *Phys. Rev. B* **49** 12431
[13] Moriarty J A, Belak J F, Rudd R E, Soderlind P, Streitz F H and Yang L H 2002 *J. Phys.: Condens. Matter* **14** 2825
[14] Soderlind P and Moriarty J A 1998 *Phys. Rev. B* **57** 10340
[15] Jakse N, Bacq O L and Pasturel A 2004 *Phys. Rev. B* **70** 174203
[16] Crowhurst J C, Zaug J M, Abramson E H, Brown J M and Ahre D W 2003 *High Pressure Res.* **23** 373
[17] Cynn H and Yoo C S 1999 *Bull. Am. Phys. Soc.* **44** 1288
[18] Antonangeli D, Farber D L, Said A H, Benedetti L R, Aracne C M, Landa A, Soderlind P and Klepeis J E 2010 *Phys. Rev. B* **82** 132101
[19] Katahara K, Manghnani M H and Fisher E S 1976 *J. Appl. Phys.* **47** 434
[20] Orlikowski D, Soderlind P and Moriarty J A 2006 *Phys. Rev. B* **74** 054109
[21] Gulseren O and Cohen R E 2002 *Phys. Rev. B* **65** 064103
[22] Koci L, Ma Y, Oganov A R, Souvatzis P and Ahuja R 2008 *Phys. Rev. B* **77** 214101
[23] Bercegeay C and Bernard S 2005 *Phys. Rev. B* **72** 214101
[24] Foata-Prestavoine M, Robert G, Nadal M and Bernard S 2007 *Phys. Rev. B* **76** 104104
[25] Shang S L, Wang Y and Liu Z K 2007 *Appl. Phys. Lett.* **90** 101909
[26] Page Y L and Saxe P 2002 *Phys. Rev. B* **65** 104104
[27] Kresse G and Furthmuller J 1996 *Phys. Rev. B* **54** 11169
[28] Kresse G and Furthmuller J 1996 *Comput. Mater. Sci.* **6** 15
[29] Zhang X D and Jiang W 2016 *Chin. Phys. B* **25** 026301
[30] Wang C J, Gu J B, Kuang X Y and Yang X D 2015 *Chin. Phys. B* **24** 086201
[31] Perdew J P, Burke K and Ernzerhof M 1997 *Phys. Rev. Lett.* **78** 1396
[32] Zhang W X, Liu Y X, Tian H, Xu J W and Feng L 2015 *Chin. Phys. B* **24** 076104
[33] Lu Q, Zhang H Y, Cheng Y, Chen X R and Ji G F 2016 *Chin. Phys. B* **25** 026401
[34] Zahra N and Aminollah V 2016 *Chin. Phys. B* **25** 037101
[35] Kresse G and Joubert D 1999 *Phys. Rev. B* **59** 1758
[36] Birch E 1978 *J. Geophys. Res.* **83** 1257
[37] Wang C J, Xiang S K, Gu J B, Kuang X Y, Yu Y, Yan X Z and Chen H Y 2014 *J. Appl. Phys.* **116** 104904
[38] Hill R 1952 *Proc. Phys. Soc. A* **65** 349
[39] Musgrave M J P 1970 *Crystal Acoustics* (San Francisco: Holden-Day)
[40] Featherston F H and Neighbours J R 1963 *Phys. Rev.* **130** 1324
[41] Manghnani M H, Katahara K and Fisher E 1974 *Phys. Rev. B* **9** 1421
[42] Dewaele A, Loubeyre P and Mezouar M 2004 *Phys. Rev. B* **69** 092106
[43] Zeng Z Y, Hu C E, Chen X R, Zhang X L, Cai L C and Jing F Q 2011 *Phys. Chem. Chem. Phys.* **13** 1669
[44] Yao Y S and Klug D D 2013 *Phys. Rev. B* **88** 054102
[45] Crowhurst J C, Zaug J M, Abramson E H, Brown J M and Ahre D W 2003 *High Pressure Res.* **23** 373
[46] Pugh S F 1954 *Philos. Mag.* **45** 823
[47] Frantsevich I N, Voronov F F and Bokuta S A 1983 *Elastic Constants and Elastic Moduli of Metals and Insulators Handbook* (I. N. Frantsevich, Naukova Dumka, Kiev)
[48] Zener C 1948 *Elasticity and Anelasticity of Metals* (Chicago: University of Chicago Press)
[49] Chung D H and Buessem W R 1967 *J. Appl. Phys.* **38** 5
[50] Antonangeli D, Krisch M, Fiquet G, Farber D L, Aracne C M, Badro J, Occelli F and Requardt H 2004 *Phys. Rev. Lett.* **93** 215505
[51] Antonangeli D, Krisch M, Farber D L, Ruddle D G and Fiquet G 2008 *Phys. Rev. Lett.* **100** 085501